

Article

Structural and Magnetic Properties of Inverse-Heusler Mn₂FeSi Alloy Powder Prepared by Ball Milling

Ondřej Životský^{1,*}, Kateřina Skotnicová², Tomáš Čegan², Jan Juřica², Lucie Gembalová¹, František Zažímal^{3,4} and Ivo Szurman²

¹ Department of Physics, Faculty of Electrical Engineering and Computer Science, VŠB—Technical University of Ostrava, 17. listopadu 2172/15, 708 00 Ostrava, Czech Republic; lucie.gembalova@vsb.cz

² Regional Materials Science and Technology Centre, Faculty of Materials Science and Technology, VŠB—Technical University of Ostrava, 17. listopadu 2172/15, 708 00 Ostrava, Czech Republic; katerina.skotnicova@vsb.cz (K.S.); tomas.cegan@vsb.cz (T.Č.); jan.jurica@vsb.cz (J.J.); ivo.szurman@vsb.cz (I.S.)

³ Institute of Physics of Materials, Czech Academy of Sciences, Žitkova 22, 616 00 Brno, Czech Republic; zazimal@ipm.cz

⁴ Department of Physical Electronics, Faculty of Science, Masaryk University, Kotlarska 267/2, 611 37 Brno, Czech Republic

* Correspondence: ondrej.zivotsky@vsb.cz; Tel.: +420-597-323-361

Abstract: Ternary Mn₂FeSi alloy was synthesized from pure elemental powders by mechanical alloying, using a high-energy planetary ball mill. The formation of an inverse-Heusler phase after 168 h of milling and subsequent annealing at 1173 K for 1.5 h was confirmed by X-ray diffraction. The diffractogram analysis yielded XA structure and the lattice parameter 0.5677 nm in a good agreement with the theoretically obtained value of 0.560 nm. The final powder was formed by particles of irregular shape and median diameter D50 of 3.8 μm and their agglomerates. The chemical analysis resulted in the mean composition of 49.0 at.% Mn, 25.6 at.% Fe and 25.4 at.% Si. At room temperature, the prepared samples featured a heterogeneous magnetic structure consisting of dominant paramagnetic phase confirmed by Mössbauer spectrometry and a weak ferro-/ferrimagnetic contribution detected by magnetization curves. From the field-cooled and zero-field-cooled curves the Néel temperature of 67 K was determined.

Keywords: inverse-Heusler alloys; ball milling; powders; microstructure; Néel temperature; magnetic transitions



Citation: Životský, O.; Skotnicová, K.; Čegan, T.; Juřica, J.; Gembalová, L.; Zažímal, F.; Szurman, I. Structural and Magnetic Properties of Inverse-Heusler Mn₂FeSi Alloy Powder Prepared by Ball Milling. *Materials* **2022**, *15*, 697. <https://doi.org/10.3390/ma15030697>

Academic Editor: Anna Bajorek

Received: 30 November 2021

Accepted: 13 January 2022

Published: 18 January 2022

Publisher's Note: MDPI stays neutral with regard to jurisdictional claims in published maps and institutional affiliations.



Copyright: © 2022 by the authors. Licensee MDPI, Basel, Switzerland. This article is an open access article distributed under the terms and conditions of the Creative Commons Attribution (CC BY) license (<https://creativecommons.org/licenses/by/4.0/>).

1. Introduction

The current rapid development of technology increases the requirements for materials research and the search for new material compositions. One of the attractive and currently investigated classes are Heusler alloys, which contain more than 4000 potential members and are applied in the fields like spintronics [1], magneto-optics [2,3], magnetoresistance and magnetocaloric devices [4,5], topological materials [6], shape memory alloys [7,8], spin injectors [9], etc. In general, regular types of Heusler materials are ternary intermetallic compounds with composition of elements X₂YZ (full-Heusler) or XYZ (half-Heusler), where X and Y are transition metals (e.g., Fe, Co, Mn) and Z is an s, p element, e.g., Si, Al, In, Sn. The full-Heusler alloy consists of two binary compounds, XY and XZ, both of CsCl type crystal structure ordered into L₂₁ or B2 structures. If two of four fcc sublattices are occupied by X atoms (Figure 1a), the X₂YZ alloy is of L₂₁ ordering in space group *Fm* $\bar{3}$ *m* (225). The Wyckoff coordinates of X elements in L₂₁ structure are (0, 0, 0) and (1/2, 1/2, 1/2), Y elements (1/4, 1/4, 1/4) and Z elements (3/4, 3/4, 3/4). If one fcc sublattice remains unoccupied the general formula XYZ represents half- or semi-Heusler alloy being of C1_b structure.

An exchange of X and Y elements in the formula of the full-Heusler alloy results in an inverse-Heusler alloy (Figure 1b) characterized by XA structure, space group $F\bar{4}3m$ (216).

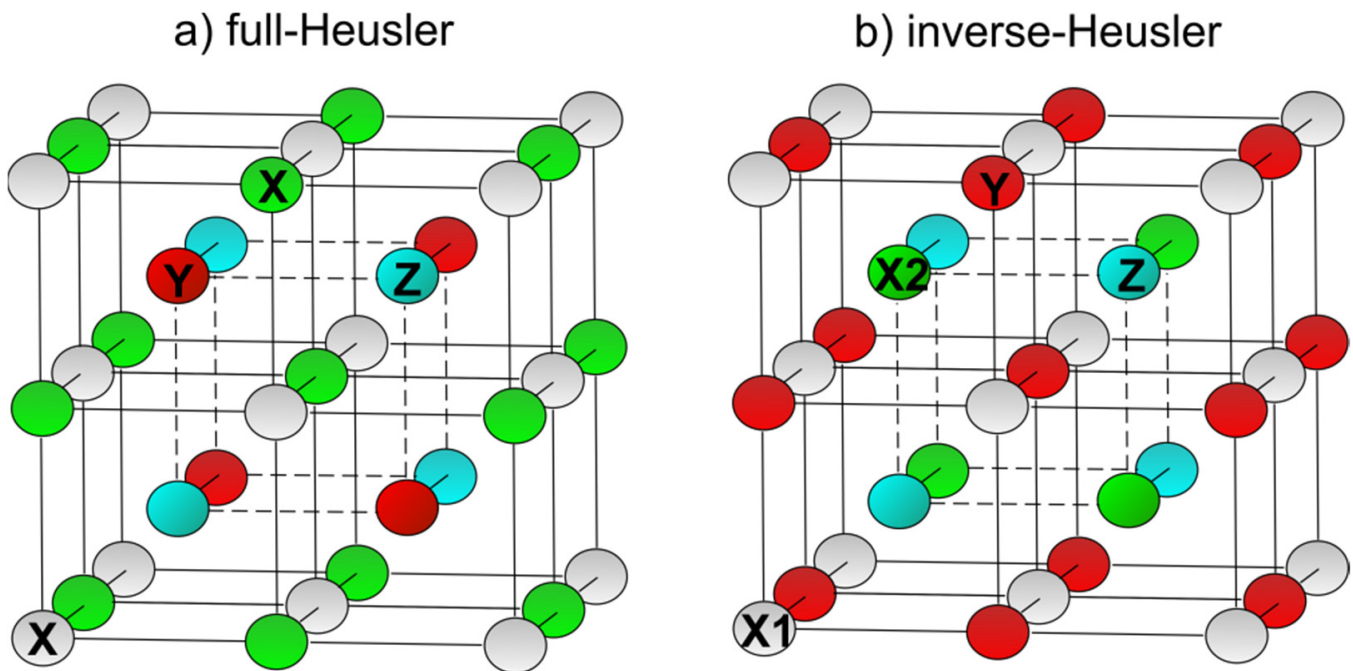


Figure 1. Unit cells formed by A, B, C and D fcc sublattices of (a) regular full-Heusler ($L2_1$) X_2YZ and (b) inverse-Heusler (XA) X_2YZ alloys. In the full-Heusler alloy $X = X_A = X_C$ (Y_B and Z_D), whereas in the inverse-Heusler alloy $X1 = X_A$ and $X2 = X_B$ (Y_C and Z_D).

Currently, two basic directions in the research of Heusler alloys can be observed. The first one is focused on the way how to synthesize these materials. In addition, the conventional techniques including arc and induction melting [10,11] producing the bulk materials, or dc- and rf-sputtering on different types of substrates in a form of thin films [12], there are still efforts for searching Heusler alloys with improved properties leading to involvement of non-traditional preparation technologies. Therefore, in last few years, there is couple of papers showing interesting properties of Heusler alloys prepared either by mechanical alloying (MA) in a form of powders [13,14] or by planar flow casting (PFC) technique having ribbon shapes [15,16]. The various ways of synthesis lead to structural imperfections on the atomic scale (antisite atoms, vacancies, etc.), different structure morphologies, different chemically ordered phases and subsequently to different physical properties determining the various applications of Heusler alloys as mentioned briefly above.

The second direction is the production of Heusler alloys with new compositions. Currently, there are many papers showing theoretical ab initio or first-principles calculations and suggesting new Heusler alloy compositions with interesting magnetic and electronic properties [17,18]. So-called inverse-Heusler alloys form one of such groups. They are characterized by a formula X_2YZ and own the XA phase in space group $F\bar{4}3m$ (216) (Figure 1b) that differs from $L2_1$ in the occupation of B and C sites. Even in this case the papers with theoretical calculations prevail [19,20] and if the alloys are produced, then mainly by mentioned conventional technologies [21,22].

The present studies are focused on the inverse-Heusler Mn_2FeSi alloys. Theoretical calculations performed on this system [19,23] determined a lattice constant of 0.560 nm, total magnetic moment of about $2 \mu_B$ /f.u. (ferrimagnetic order, half-metallicity) and relatively large and antiparallel Mn moments at sites A and B. Experimentally, this alloy has so far been prepared only in the form of ingots and thin films [21,24]. However, observed antiferromagnetic behavior at low temperatures contradicts theoretical calculations and

refers to the need for further detailed research [25]. This paper is focused on the Mn_2FeSi alloy prepared by mechanical alloying into a powder form and on its detail structural and physical characterization. For this purpose, the X-ray diffraction, electron microscopy, Mössbauer spectrometry and room- and low-temperature magnetic measurements are used and the results are compared with experimental and theoretical literature data.

2. Materials and Methods

2.1. Materials

The powders of manganese (≥ 99.3 wt.%), iron (≥ 99.5 wt.%) and silicon (99.9985 wt.%) from Alfa Aesar (Massachusetts, USA) were used as raw materials. The data on particle size distribution of these powders are given in Table 1. The Mn:Fe:Si ratio was 50:25:25 (in at.%).

Table 1. Particle size distributions of starting Mn, Fe and Si powders.

Element	D10 (μm)	D50 (μm)	D90 (μm)
Mn	5.6	29.8	67.6
Fe	2.9	6.4	14.0
Si	1.0	5.5	16.8

2.2. Synthesis

The inverse-Heusler Mn_2FeSi alloy was synthesized by mechanical alloying using ball milling followed by thermal treatment. Mn, Fe and Si powders were initially mixed using the Turbula T2F mixer (Willy A. Bachofen AG, Muttenz, Switzerland) rotated at 50 rpm for 15 min. The powder mixture with initial weight of 50 g (56.7 wt.% Mn, 28.8 wt.% Fe, 14.5 wt.% Si) was placed in a stainless-steel milling bowl together with stainless-steel balls of 5 mm in diameter. The ball-to-powder weight ratio was 10:1. The n-hexane was added as the solvent in order to reduce the surface energy of particles and achieve a small particle size as well as good homogeneity. The milling bowl was sealed, evacuated several times and then filled with argon gas (99.999%). The process was realized using a high-energy ball mill E-max (Retsch GmbH, Haan, Germany) at 500 rpm for 168 h. Controlled integrated water cooling of milling bowl was used during milling. The alloying process was checked after selected times of milling. The pure elements were still observed after 80 h of milling as it is shown in Figure 2. Nevertheless, after 168 h of milling no pure elements were detected but the X-ray diffraction (XRD) measurement did not show any typical pattern expected for Mn_2FeSi alloy. On the contrary, only a few sharper peaks next to broad amorphous halo were seen. This was caused by a presence of n-hexane used during milling. Therefore, a small amount of powder was thermally treated (1173 K/1.5 h) to remove solvent which was confirmed by repeated XRD measurement. The same annealing conditions, 1173 K/1.5 h and the dynamic argon atmosphere with flow rate 2 L/min, in a high-temperature sintering furnace (Xerion Advanced Heating[®] Ofentechnik GmbH, Berlin, Germany) were subsequently used to form final (annealed) Mn_2FeSi alloy.

2.3. X-ray Diffraction Analysis

The crystal structure and phase composition of powders were studied by powder X-ray diffraction. The XRD diffractometer AXS D8 Advance (Bruker AXS GmbH, Karlsruhe, Germany) equipped with the position-sensitive LynxEye detector and $\text{CuK}\alpha$ radiation at room temperature (RT) was used for measurements in the range $2\theta = 20^\circ - 95^\circ$, steps 0.014° and time per step 2 s. The qualitative and quantitative analyses of diffractograms were performed using the Rietveld method.

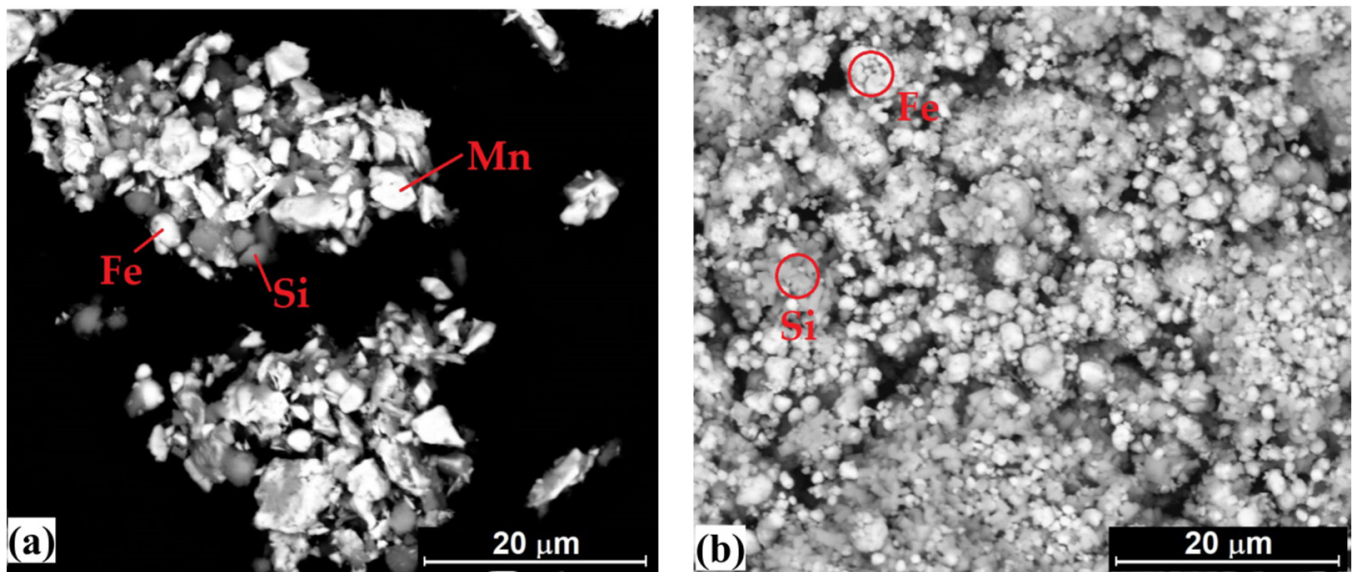


Figure 2. The particle morphology of Mn-Fe-Si powder after 1 h (a) and 80 h (b) of milling.

2.4. Microstructural Characterization and Particle Size Distribution

The microstructure, chemical composition and element mapping were studied by scanning electron microscopy (SEM) using a QUANTA 450 FEG (FEI Company, Hillsboro, OR, USA) equipped with an energy-dispersive X-ray (EDX) APOLLO X analyser. The images were taken in the backscattered electron mode (BSE). The particle size distribution was measured by laser diffraction particle size analyser MasterSizer 3000 (Malvern Panalytical Ltd., Malvern, UK).

2.5. Mössbauer and Magnetic Measurements

Mössbauer spectrometry (MS) measurements were performed in transmission geometry by γ -rays at RT using a ^{57}Co (Rh) source. Calibration of the velocity scale was done with α -Fe at RT and the isomer shifts are given with respect to its Mössbauer spectrum. All spectra were evaluated using the transmission integral approach in the program CONFIT [26]. The experimental points were analysed by the double- and/or single-line components yielding values of isomer shift (δ) and quadrupole splitting (Δ). The relative representations of these subcomponents are denoted by A.

Magnetic properties were obtained using a vibrating sample magnetometer (VSM) EZ9 (Microsense, Lowell, MA, USA) and a Physical Property Measurement System (PPMS, Model P935A, San Diego, CA, USA) Quantum Design. VSM was used for measurements of room- and high-temperature magnetization curves with maximal applied magnetic field of ± 1600 kA/m (± 2 T). PPMS was applied for low-temperature experiments, these are (i) magnetization curves at chosen constant temperatures with maximal magnetic field of ± 2400 kA/m (± 3 T) and (ii) field-cooled (FC) and zero-field-cooled (ZFC) curves measured in the temperature range 2–293 K at a magnetic field of 80 kA/m.

3. Results and Discussion

3.1. Morphology, Phase and Chemical Composition

The particle morphologies of initial manganese, iron and silicon powders are shown in Figure 3. Mn powder consisted of irregular polyhedral particles with sharp edges. Fe powder is characterized by a nearly spherical shape of particles with smooth surface. Si powder was typical by the irregular shaped particles with rough surface and high porosity. The annealed Mn_2FeSi alloy powder (Figure 4) was characterized by the irregular shape of particles and bimodal distribution with peaks at 2.9 μm and 13.6 μm , respectively. Its median particle diameter D50 reached a value of 3.8 μm .

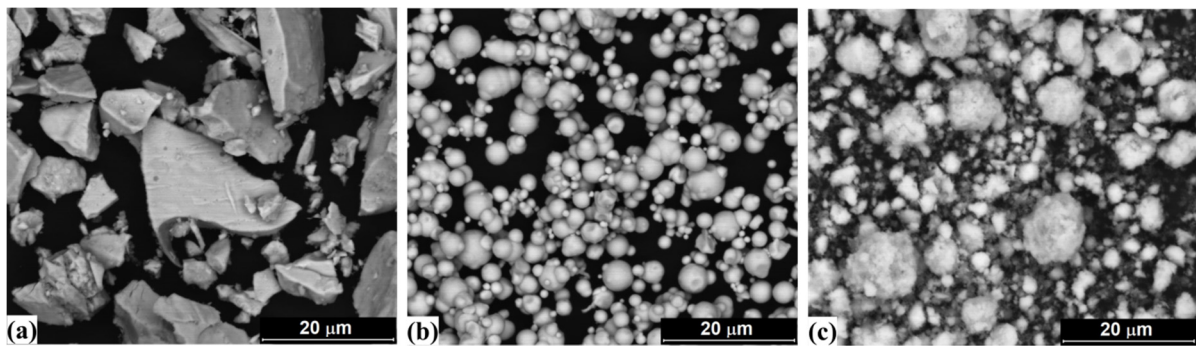


Figure 3. The particle morphologies of initial powders: (a) Mn, (b) Fe, (c) Si (SEM/BSE).

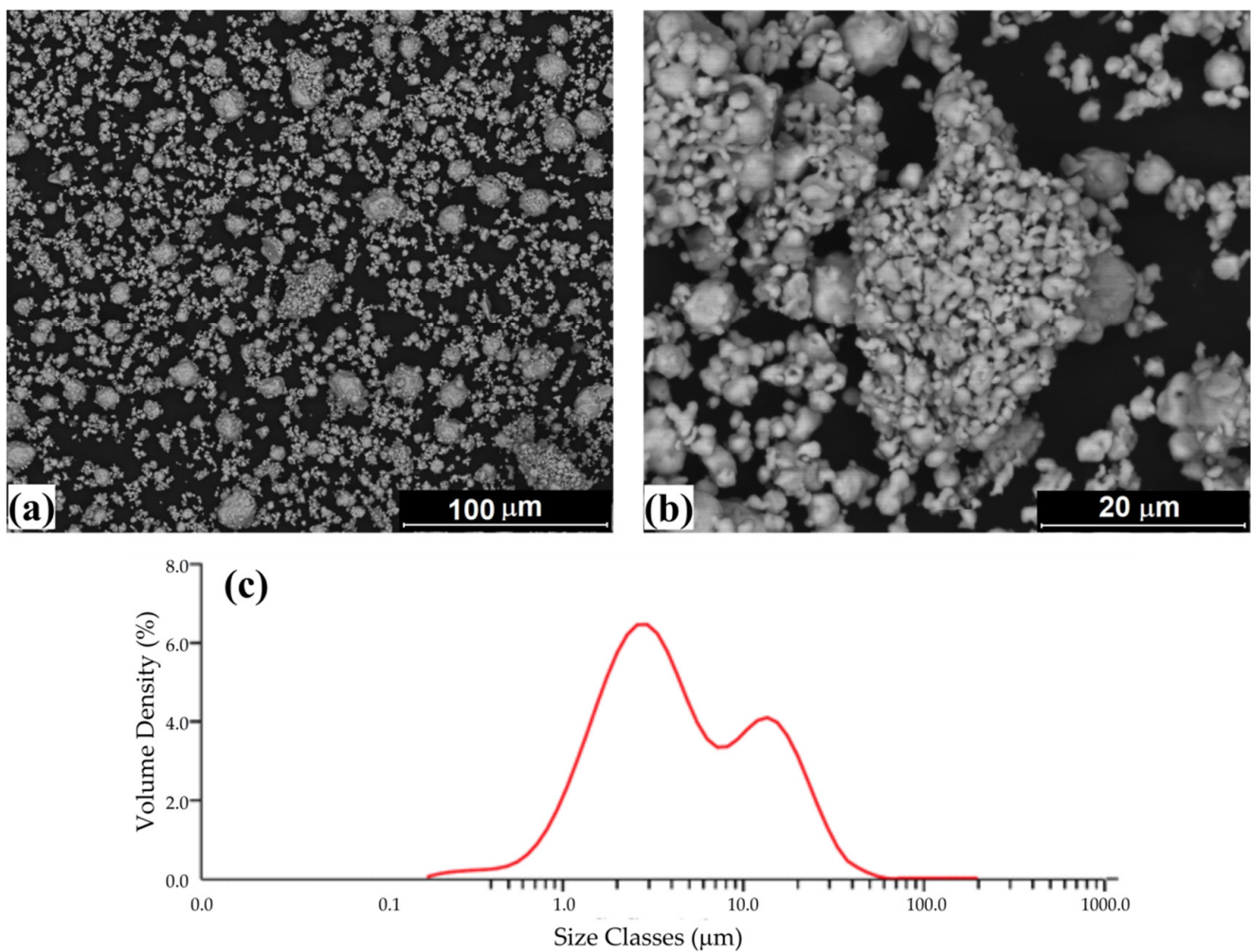
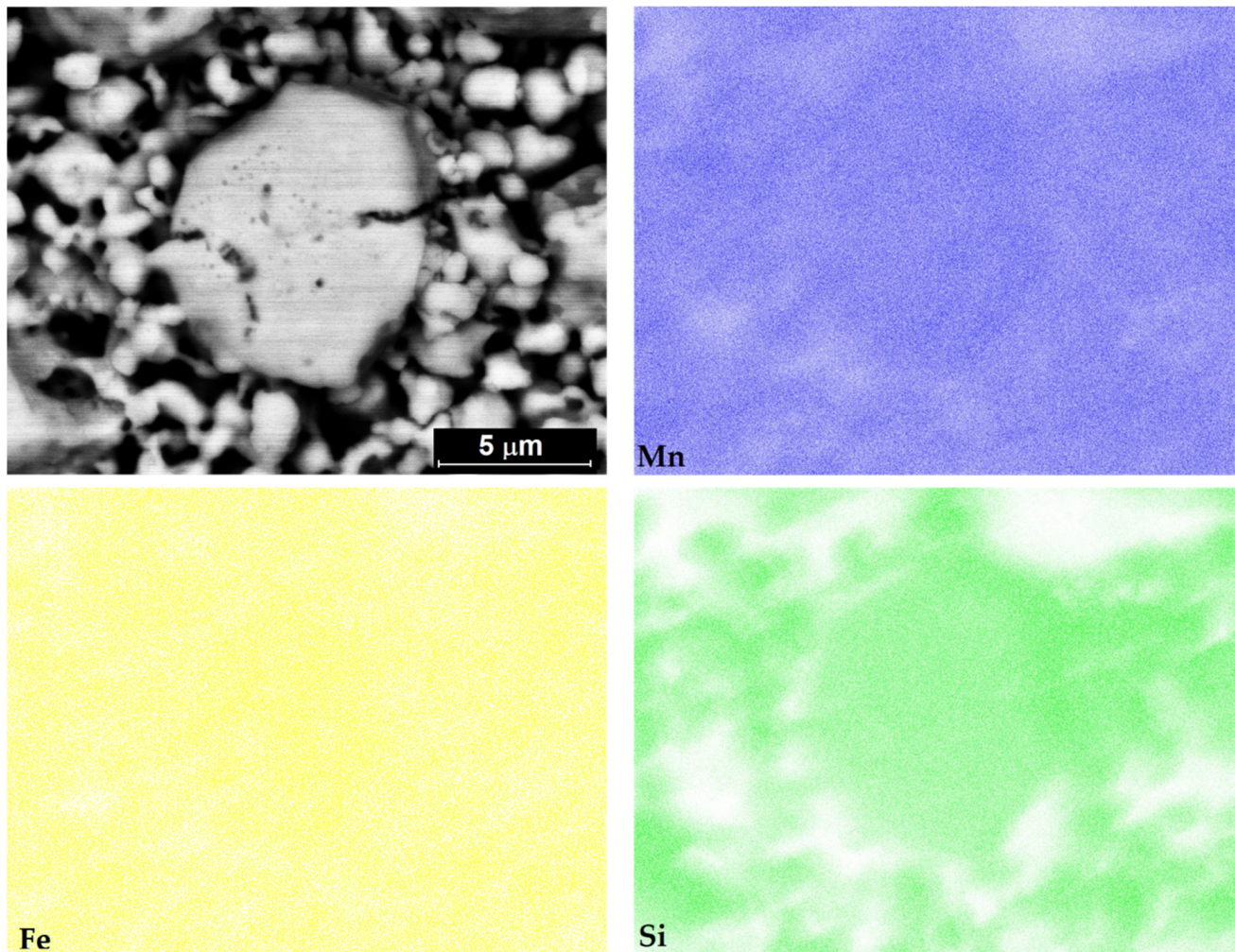


Figure 4. (a,b) The particle morphology of inverse-Heusler Mn_2FeSi alloy powder (SEM/BSE) and (c) its particle size distribution with bimodal character.

The chemical composition of the final Mn_2FeSi powder, determined from the volume of particles (i.e., metallographic cut of powder sample was prepared), is summarized in Table 2 as averaged values from seven-spot EDX analysis. It can be seen that the chemical composition corresponds very well to the nominal composition of the alloy. The distribution of Mn, Fe and Si, investigated using the X-ray element mapping, is uniform throughout the particle volume and no obvious inhomogeneities were observed (see Figure 5).

Table 2. The average chemical composition of inverse-Heusler Mn₂FeSi alloy powder.

Mn (at.%)	Fe (at.%)	Si (at.%)
49.0 ± 0.8	25.6 ± 1.0	25.4 ± 1.5

**Figure 5.** X-ray maps showing the distribution of Mn, Fe and Si in the particle of annealed Mn₂FeSi alloy powder.

X-ray diffraction patterns in Figure 6 show visible difference between the as-milled (a) and annealed (b) states of samples. The diffractogram of as-milled powder (Figure 6a) contains broad halos between 30° and 40° and similarly at higher 2θ angles, that next to only few sharp peaks come from the organic n-hexane used during milling. Consequently, these halos diminish after the sample annealing and the Rietveld analysis of its diffractogram (Figure 6b) evidences cubic Heusler alloy with the lattice parameter 0.5677 nm well agreed with the theoretical value 0.560 nm of Mn₂FeSi alloy [18,22]. Generally, it is not simple to distinguish the inverse- and full-Heusler structure in their diffractograms. Nevertheless, the theoretical simulations yield higher relative intensity of the (111) diffraction peak compared to (200) for the inverse-Heusler alloy of XA structure [21]. Based on this result, the pattern in Figure 6b confirms formation of the inverse-Heusler Mn₂FeSi alloy. Next to peaks characterizing the produced Heusler alloy, the peaks at positions 35°, 41° and 43° reflect; moreover, a presence of not specified impurity phase formed during the alloying

process. It could be iron and/or manganese oxides speculatively identified from Mössbauer spectrum analysis based on Ref. [27] and presented below.

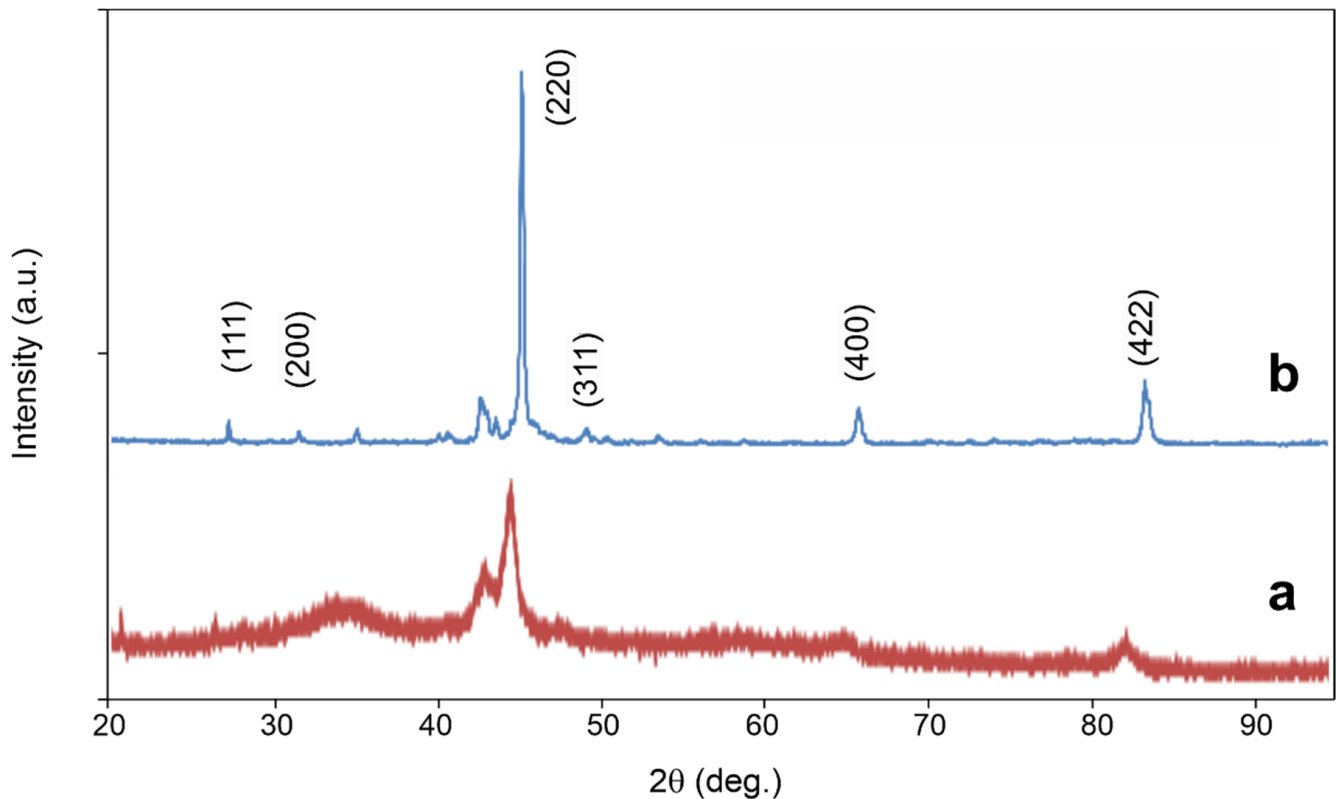


Figure 6. X-ray diffraction pattern of Mn_2FeSi alloy powder milled for 168 h (a) and annealed at 1173 K for 1.5 h (b).

3.2. Magnetic and Mössbauer Results

Figure 7 shows the room temperature Mössbauer spectrum (a) and magnetization curves of the annealed Mn_2FeSi alloy powder measured at room and elevated temperatures (b). The experimental points (x) of the Mössbauer spectrum were analysed using single-line (singlet) and two-line (doublet) subcomponents of different intensities and different hyperfine parameters summarized in Table 3. The main contribution of the singlet (53.6%) represents a paramagnetic Mn_2FeSi phase while doublets can be speculatively ascribed to a nonstoichiometric (Fe,Mn)-oxides and/or to chemical disorder at agglomerate boundaries. No presence of ferromagnetic component was identified by this Mössbauer measurement.

RT magnetization curve (Figure 7b, 303 K) is not saturated and shows linear dependence of magnetization on an applied external magnetic field H for $H > \pm 150$ kA/m. This confirms paramagnetic nature of the alloy powder being in full agreement with Mössbauer analysis. However, magnetization reversal in the low external magnetic field, $H < \pm 150$ kA/m, characterized by nonzero remanent magnetization, $M_r \approx 0.015$ Am²/kg, and coercivity, $H_c \approx 4$ kA/m, reflects a presence of a small contribution of ferro- and/or ferrimagnetic (distorted) phase. Heterogeneous magnetic behavior is observed also on magnetization curves at elevated temperatures, whereas magnitudes of M_r and H_c parameters decrease with increasing temperature.

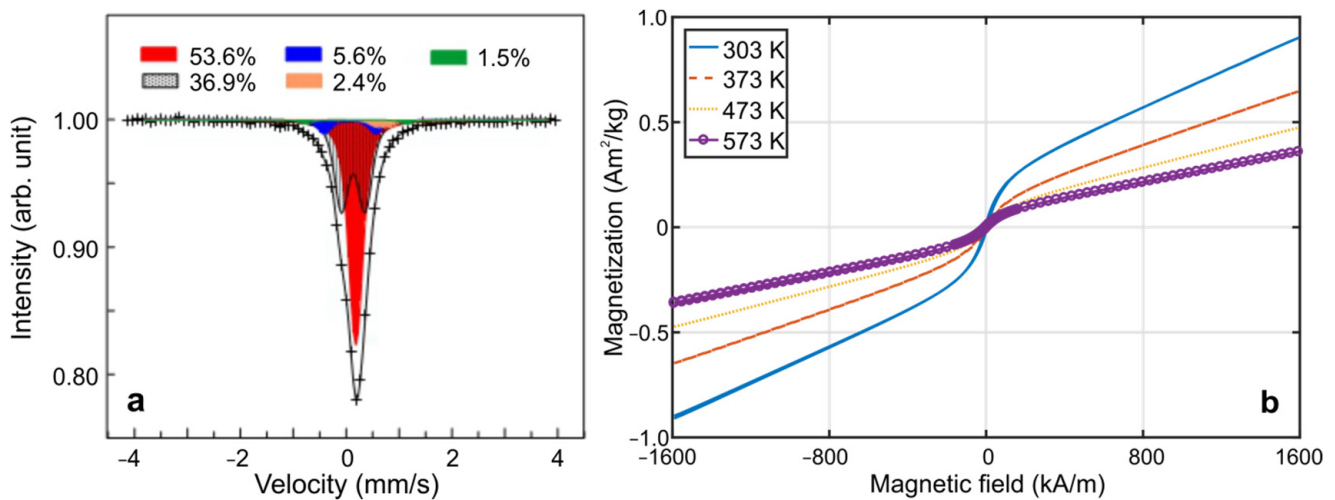


Figure 7. (a) Room temperature Mössbauer spectrum. (b) Magnetization curves of the annealed Mn_2FeSi powder at room and elevated temperatures.

Table 3. Hyperfine parameters, isomer shift, δ , quadrupole splitting, Δ and relative intensity, A , of annealed Mn_2FeSi powder.

Component	δ (mm/s)	Δ (mm/s)	A (%)
S (singlet)	0.181(1)		53.6(5)
D1 (doublet)	0.133(3)	0.445(7)	36.9(4)
D2	0.078(16)	0.974(33)	5.6(3)
D3	0.696(26)	0.261(33)	2.4(5)
D4	0.196(26)	1.922(56)	1.5(2)

The low-temperature magnetic measurements of inverse-Heusler Mn_2FeSi alloy powder are presented in Figure 8. The FC and ZFC curves shown in Figure 8a detect low magnetization of alloys when cooled from room temperature to about 170 K. The magnetic behavior is similar to that at room temperature and the magnetization curves in this temperature range (Figure 8b, 200 K) consist of a weak magnetization reversal at low magnetic fields and linear contribution at higher fields.

The FC and ZFC curves separate at approximately 155 K. This temperature corresponds to the inflection point of both curves and can be denoted as the thermodynamic temperature of a transition to ferro-/ferrimagnetic state. We suppose that splitting of the FC/ZFC curves is not caused by the distorted phase, but by the impurities that exhibit dynamic behavior similar to the superparamagnetic systems. As a consequence, a more pronounced increase of remanent magnetization and coercive field is seen (Figure 8c). Therefore, the superposition of two magnetic contributions below 155 K, namely, ferro-/ferrimagnetic phase and disordered phase, is expected. Detailed analyses of the magnetization and FC-ZFC curves reveal an increase of disordered phase contribution during cooling below 155 K.

The decrease of disordered phase occurs only after exceeding the temperature of 67 K, which corresponds to the Néel temperature, T_N , below which the alloy exhibits an antiferromagnetic behavior. Contrary, the ferro-/ferrimagnetic phase represented by the coercive field and remanent magnetization continue to increase even during cooling to 2 K. The highest value of magnetization at a temperature of 2 K and a magnetic field of 2400 kA/m is about $12 \text{ Am}^2/\text{kg}$. Generally, the theoretically predicted magnetic structure giving the lowest total energy for the XA crystallographic structure at zero temperature is ferrimagnetic. However, experimentally confirmed antiferromagnetic behavior can be realized in tetragonal or cubic (frustrated) crystallographic structures.

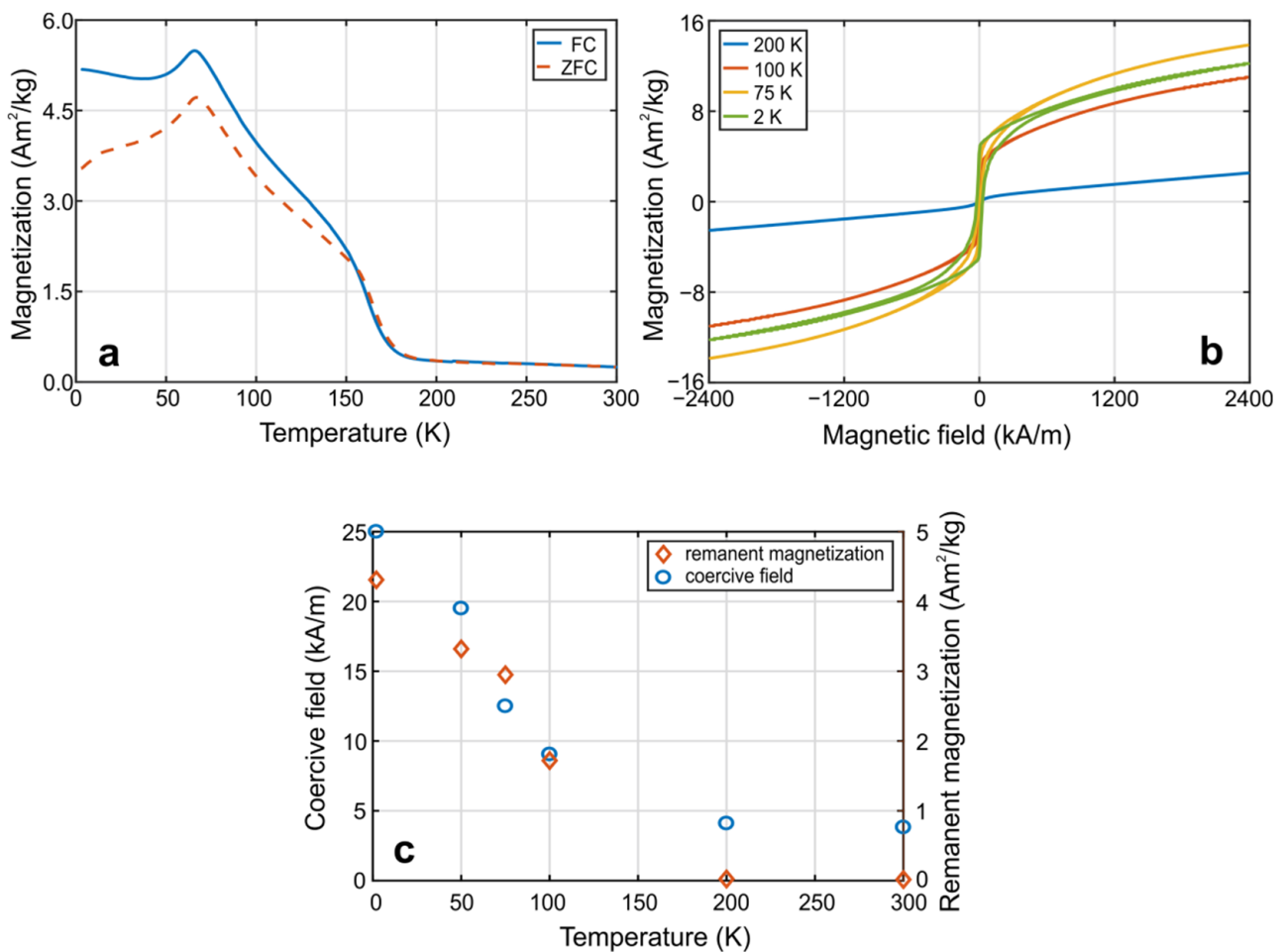


Figure 8. Low-temperature magnetic properties of annealed Mn_2FeSi powder sample. (a) Field-cooled (FC) and zero-field-cooled (ZFC) curves at a constant magnetic field of 80 kA/m, (b) magnetization curves at different temperatures, (c) coercive field and remanent magnetization as a function of temperature.

Magnetic properties of prepared Mn_2FeSi alloy powder are different from annealed ingots (773 K/48 h) and powders (1223 K/100 h) presented in the literature [21,28]. Both systems exhibit antiferromagnetic-paramagnetic transition at T_N about 50 K. However, it can be seen from Ref. [28] that an increase in the amount of Fe at the expense of Mn can significantly change the magnetic behavior of the alloy powder. For example, the system $Mn_{1.5}Fe_{1.5}Si$ [28] shows antiferromagnetic-ferromagnetic-paramagnetic transitions with Néel temperature at 62 K and Curie temperature at 137 K, but the shape of the FC-ZFC curves in the ferromagnetic region is completely different from that in Figure 8a, where we suppose superposition of ferro-/ferrimagnetic and paramagnetic contributions (67–155 K). Thus, it seems that the final magnetic properties will depend not only on the composition of the alloy, but also on the temperature and annealing time, which is significantly shorter (1.5 h) in the currently prepared alloy powders.

4. Conclusions

The present work is devoted to the microstructural and magnetic investigations of Mn_2FeSi alloy prepared from pure elemental powders by mechanical alloying. The formation of the inverse-Heusler (XA) phase with the corresponding lattice parameter (0.5677 nm) required ball milling for 168 h in the presence of solvent (n-hexane) and subsequent annealing in a sintering furnace at 1173 K for 1.5 h in a protective argon atmosphere. SEM/EDX and particle size distribution analyses of the annealed powder indicated practically no

deviations from the nominal composition, irregular shape of particles having bimodal distribution with peaks at 2.9 μm and 13.6 μm and median particle diameter D50 of 3.8 μm .

Magnetic measurements revealed heterogeneous magnetic behavior of the final alloy. In the temperature range from 170 K to 573 K we detected the dominant paramagnetic (disordered) phase and a small ferro-/ferrimagnetic contribution showing magnetization reversal and nonzero values of remanent magnetization M_r and coercive field H_c on measured magnetization curves. Below 155 K, the step increase of M_r and H_c and the splitting of the FC and ZFC curves are observed. A decrease in the disordered phase contribution is found after the system has cooled below 67 K. This is reflected in the maximum of the FC and ZFC curves at 67 K that probably corresponds to the Néel temperature below which the antiferromagnetic arrangement of the spins originates.

The present investigations have evidenced a possibility to prepare the inverse-Heusler Mn_2FeSi alloy using mechanical alloying. Nevertheless, several open questions as, e.g., an origin of the ferro-/ferrimagnetic phase, its effect on the magnetic behavior of the pure inverse-Heusler Mn_2FeSi , the reason why it was not detected by highly sensitive Mössbauer spectrometry, the real influence of producing technology, etc., remain for the future investigations.

Author Contributions: Conceptualization, O.Ž.; methodology, K.S., T.Č., J.J. and I.S.; investigation, O.Ž., K.S., T.Č., L.G. and F.Z.; data curation, O.Ž., K.S., L.G. and F.Z.; writing—draft preparation, O.Ž.; writing—review and editing, K.S. and L.G. All authors have read and agreed to the published version of the manuscript.

Funding: This work was funded by the Czech Science Foundation under the project No. 21-05339S, by the Ministry of Education, Youth, and Sports of the Czech Republic via the project SP2021/64 and by the Czech academy of Sciences via the project UFM-A-RVO:68081723.

Institutional Review Board Statement: Not applicable.

Informed Consent Statement: Not applicable.

Data Availability Statement: The data presented in this study are available on request from the corresponding author.

Acknowledgments: Special thanks are given to Y. Jiraskova from the Institute of Physics of Materials, AS CR, for the Mössbauer data analysis.

Conflicts of Interest: The authors declare no conflict of interest.

References

1. Chatterjee, S.; Chatterjee, S.; Giri, S.; Majumdar, S. Transport properties of Heusler compounds and alloys. *J. Phys. Condens. Matter* **2022**, *34*, 013001. [[CrossRef](#)] [[PubMed](#)]
2. Silber, R.; Kral, D.; Stejskal, O.; Kubota, T.; Ando, Y.; Pistora, J.; Veis, M.; Hamrle, J.; Kuschel, T. Scaling of quadratic and linear magneto-optic Kerr effect spectra with L2(1) ordering of Co_2MnSi Heusler compound. *Appl. Phys. Lett.* **2020**, *116*, 262401. [[CrossRef](#)]
3. Kral, D.; Beran, L.; Zeleny, M.; Zemen, J.; Antos, R.; Hamrle, J.; Zazvorka, J.; Rames, M.; Onderkova, K.; Heczko, O.; et al. Magnetic and Magneto-Optical Properties of $\text{Fe}_{75-x}\text{Mn}_{25}\text{Ga}_x$ Heusler-like Compounds. *Materials* **2020**, *13*, 703. [[CrossRef](#)]
4. Chabri, T.; Barman, A.; Chatterjee, S.; Mollick, S.A.; Nath, T.K.; Mukherjee, D. Effects of transitional hysteresis on the large magnetocaloric and magnetoresistance properties of Ni-Mn-Co-Sn Heusler alloy. *J. Alloys Compd.* **2021**, *863*, 158485. [[CrossRef](#)]
5. Mukhopadhyay, A.; Singh, K.; Sen, S.; Mukherjee, K.; Nayak, A.K.; Mohapatra, N. Anomalous magnetoresistance and magneto-thermal properties of the half-Heuslers, RPdSi ($R = \text{Y}, \text{Gd-Er}$). *J. Phys. Condens. Matter* **2021**, *33*, 435804. [[CrossRef](#)]
6. Zhang, W.; Balasubramanian, B.; Sun, Y.; Ullah, A.; Skomski, R.; Pahari, R.; Valloppilly, S.R.; Li, X.-Z.; Wang, C.-Z.; Ho, K.-M.; et al. Magnetism and topological Hall effect in antiferromagnetic Ru_2MnSn -based Heusler compounds. *J. Magn. Magn. Mater.* **2021**, *537*, 168104. [[CrossRef](#)]
7. Bachaga, T.; Zhang, J.; Khitouni, M.; Sunol, J.J. NiMn-based Heusler magnetic shape memory alloys: A review. *Int. J. Adv. Manuf. Technol.* **2019**, *103*, 2761–2772. [[CrossRef](#)]
8. Czaja, P.; Chulist, R.; Wierzbicka-Miernik, A.; Brzozka, A.; Fitta, M.; Maziarz, W. Microstructure evolution and magnetic properties in Mn-rich Ni-(Co, Cu, Fe)-Mn-Sn Heusler base shape memory alloys. *Mater. Chem. Phys.* **2019**, *235*, 121720. [[CrossRef](#)]
9. Sasaki, Y.; Sugimoto, S.; Takahashi, Y.K.; Kasai, S. Spin injection efficiency through the pumping in epitaxial $\text{Co}_2\text{MnSi}/\text{Pt}$ thin film. *AIP Adv.* **2020**, *10*, 085311. [[CrossRef](#)]

10. Jiraskova, Y.; Pizurova, N.; Titov, A.; Janickovic, D.; Friak, M. Phase separation in Fe-Ti-Al alloy—Structural, magnetic, and Mössbauer study. *J. Magn. Magn. Mater.* **2018**, *468*, 91–99. [CrossRef]
11. Titov, A.; Jiraskova, Y.; Zivotsky, O.; Bursik, J.; Janickovic, D. Microstructure and magnetism of Co₂FeAl Heusler alloy prepared by arc and induction melting compared with planar flow casting. *AIP Adv.* **2018**, *8*, 047206. [CrossRef]
12. Huminiuc, T.; Whear, O.; Vick, A.J.; Lloyd, D.C.; Vallejo-Fernandez, G.; O'Grady, K.; Hirohata, A. Growth and Characterisation of Antiferromagnetic Ni₂MnAl Heusler Alloy Films. *Magnetochemistry* **2021**, *7*, 127. [CrossRef]
13. Ahmad, A.; Mitra, S.; Srivastava, S.K.; Das, A.K. Size-dependent structural and magnetic properties of disordered Co₂FeAl Heusler alloy nanoparticles. *J. Magn. Magn. Mater.* **2019**, *474*, 599–604. [CrossRef]
14. Nehla, P.; Ulrich, C.; Dhaka, R.S. Investigation of the structural, electronic, transport and magnetic properties of Co₂FeGa Heusler alloy nanoparticles. *J. Alloys Compd.* **2019**, *776*, 379–386. [CrossRef]
15. Li, X.Z.; Zhang, W.Y.; Valloppilly, S.; Sellmyer, D.J. New Heusler compounds in Ni-Mn-In and Ni-Mn-Sn alloys. *Sci. Rep.* **2019**, *9*, 7762. [CrossRef] [PubMed]
16. Zivotsky, O.; Bursik, J.; Janickovic, D.; Titov, A.; Jiraskova, Y. Low-temperature magnetic transitions in Fe₂MnSi Heusler alloys prepared in bulk and ribbon form. *J. Magn. Magn. Mater.* **2019**, *475*, 5–9. [CrossRef]
17. Masrour, R.; Jabar, A.; Labidi, S.; El Krimi, Y.; Ellouze, M.; Labidi, M.; Amara, A. Study of structural, elastic, thermal, electronic and magnetic properties of heusler Mn₂NiGe: An Ab initio calculations and Monte Carlo simulations. *Mater. Today Commun.* **2021**, *26*, 101772. [CrossRef]
18. Hao, Z.P.; Liu, R.; Fan, Y.H.; Wang, L.L. First-principles calculations of a new half-metallic Heusler alloy FeCrAs. *J. Alloys Compd.* **2020**, *820*, 153118. [CrossRef]
19. Ma, J.; He, J.; Mazumdar, D.; Munira, K.; Keshavarz, S.; Lovorn, T.; Wolverton, C.; Ghosh, A.W.; Butler, W.H. Computational investigation of inverse Heusler compounds for spintronics applications. *Phys. Rev. B* **2018**, *98*, 094410. [CrossRef]
20. Lalrinkima; Ekuma, C.E.; Chibueze, T.C.; Fomin, L.A.; Malikov, I.V.; Zadeng, L.; Rai, D.P. Electronic, magnetic, vibrational, and X-ray spectroscopy of inverse full-Heusler Fe₂IrSi alloy. *Phys. Chem. Chem. Phys.* **2021**, *23*, 11876–11885. [CrossRef]
21. Aryal, A.; Bakkar, S.; Samassekou, H.; Pandey, S.; Dubenko, I.; Stadler, S.; Ali, N.; Mazumdar, D. Mn₂FeSi: An antiferromagnetic inverse-Heusler alloy. *J. Alloys Compd.* **2020**, *823*, 153770. [CrossRef]
22. Xu, X.D.; Chen, Z.X.; Sakuraba, Y.; Perumal, A.; Masuda, K.; Kumara, L.S.; Tajiri, H.; Nakatani, T.; Wang, J.; Zhou, W.; et al. Microstructure, magnetic and transport properties of a Mn₂CoAl Heusler compound. *Acta Mater.* **2019**, *176*, 33–42. [CrossRef]
23. Luo, H.Z.; Zhang, H.W.; Zhu, Z.Y.; Ma, L.; Xu, S.F.; Wu, G.H.; Zhu, X.X.; Jiang, C.B.; Xu, H.B. Half-metallic properties for the Mn₂FeZ (Z = Al, Ga, Si, Ge, Sb) Heusler alloys: A first-principles study. *J. Appl. Phys.* **2008**, *103*, 083908. [CrossRef]
24. Granovskii, A.B.; Soboleva, E.A.; Fadeev, E.A.; Dubenko, I.S.; Aryal, A.; Samassekou, H.; Pandey, S.; Stadler, S.; Mazumdar, D.; Lahderanta, E. Martensitic Phase Transition in Magnetic Thin Films Based on Inverse Mn₂FeSi Heusler Alloys. *J. Exp. Theor. Phys.* **2020**, *130*, 117–122. [CrossRef]
25. Draganyuk, O.N.; Zhandun, V.S.; Zamkova, N.G. Half-metallicity in Fe₂MnSi and Mn₂FeSi heusler compounds: A comparative ab initio study. *Mater. Chem. Phys.* **2021**, *271*, 124897. [CrossRef]
26. Zak, T.; Jiraskova, Y. CONFIT: Mössbauer spectra fitting program. *Surf. Interface Anal.* **2006**, *38*, 710. [CrossRef]
27. Bakkar, S. New inverse-Heusler materials with potential spintronics applications. *Thesis* **2017**, *2207*, 44–50. Available online: <http://opensiuc.lib.siu.edu/theses/2207> (accessed on 12 January 2022).
28. Leitão, J.V.; Xinmin, Y.; Caron, L.; Brück, E. Magnetostructural study of the (Mn,Fe)₃(P, Si) system. *J. Alloys Compd.* **2012**, *520*, 52–58. [CrossRef]